



Article

# Mechanical Properties of Uncured Thermoset Tow Prepreg: Experiment and Finite Element Analysis

Mina Derakhshani Dastjerdi \*, Massimo Carboni and Mehdi Hojjati

Department of Mechanical, Industrial, and Aerospace Engineering, Concordia University, 1455 De Maisonneuve Blvd W., Montreal, QC H3G 1M8, Canada; carboni.mass@gmail.com (M.C.); mehdi.hojjati@concordia.ca (M.H.)  
\* Correspondence: minaderakhshani.92@gmail.com

**Abstract:** This paper presents an experimental analysis of the tensile behavior of unidirectional carbon/epoxy prepreg, focusing on the nonlinearity observed at the beginning of the stress–strain curve. Due to the material’s high viscosity, securely holding specimens during testing was challenging, prompting modifications in the gripping method to ensure reliable data. By using a longer gauge length, the slippage impact on elastic modulus measurement was minimized, resulting in good repeatability among the test samples. Experimental findings highlighted the significant interaction between fiber waviness and the viscous matrix, leading to stiffness reduction. The linear stiffness of the samples closely matched that of the fibers and remained unaffected by temperature variations. However, at higher temperatures, the epoxy matrix’s decreased viscosity caused an upward shift in the stiffness plot within the non-linear region. To support the experimental findings, a micromechanical model of prepreg tow with fiber waviness was proposed. An RVE model of periodically distributed unidirectional waved cylindrical fibers embedded within the matrix was developed to predict effective material stiffness parameters. The simulation outcomes aligned well with the uniaxial tensile test of the prepreg tow, demonstrating the proposed RVE model’s capability to accurately predict elastic properties, considering factors like fiber arrangement, waviness, and temperature.

**Keywords:** tensile modulus; prepreg; fiber waviness; RVE



**Citation:** Derakhshani Dastjerdi, M.; Carboni, M.; Hojjati, M. Mechanical Properties of Uncured Thermoset Tow Prepreg: Experiment and Finite Element Analysis. *J. Compos. Sci.* **2023**, *7*, 312. <https://doi.org/10.3390/jcs7080312>

Academic Editor: Stelios K. Georgantzinos

Received: 23 June 2023  
Revised: 19 July 2023  
Accepted: 27 July 2023  
Published: 29 July 2023



**Copyright:** © 2023 by the authors. Licensee MDPI, Basel, Switzerland. This article is an open access article distributed under the terms and conditions of the Creative Commons Attribution (CC BY) license (<https://creativecommons.org/licenses/by/4.0/>).

## 1. Introduction

Various manufacturing techniques have been developed for composites, such as automated tow laying ATL, automated fiber placement AFP, and compression molding. Their main objectives are to automate the process, reduce production cycle cost/time, and improve production cycle part quality. Yet, uncertainties in material behavior and processing conditions can lead to overdesigned parts and, consequently, to increasing weight and cost. So, many designers prefer using conventional bulk materials with predictable mechanical behaviors. Therefore, software tools are needed to provide better process modeling and material characterization [1,2].

AFP and ATL manufacturing techniques rely on process modeling simulations to predict the path of the fibers and control the process parameters to avoid defect formation. This process model is used to simulate the machine head path to predict how the prepreg will be laid down and can also be used to control and predict tape overlap/gap, tow buckling, and wrinkle formation [3,4]. One of the limiting factors in process modeling for AFP and ATL is the reliance on using the cured composite material properties when the material properties for the uncured state are required, as well as assuming ideal properties associated with the straight fiber material. Variability exists in the material properties between both states, with the properties of the uncured state being significantly lower due to the viscous matrix. Furthermore, such properties are generally nonconservative because stiffness and strength are usually lower than what is predicted by the straight fiber models [5].

Several studies have been conducted on the characterization of the bending behavior of prepregs [6–9]; however, only a few studies have been done to investigate the tensile properties of prepregs. Potter et al. [10,11] carried out tensile tests of UD prepreg tapes and reported a considerable nonlinearity in the beginning of the stress–strain curve of all cases due to the fiber waviness and the resistance the fibers are experiencing as they move through the highly viscous resin. Zhang et al. [12] performed uniaxial tests on woven prepreg at temperatures varying between 23 °C and 80 °C. They studied the effects of temperature on the nonlinear section of the stress–strain plot and determined that, as temperature increases, the area of nonlinearity also increases, and the tensile modulus for the settle-down region slightly reduces. However, the phenomenon and the reasoning behind the effects on the non-linear region were not addressed. Furthermore, they selected the stiffness represented by the linear section of the plot to describe the response of the uncured prepreg. A similar test method was conducted by Sentis et al. [13] in their study of the tensile behavior of uncured sheet molding compounds. Dangora et al. [1] performed tensile tests on strips of thermoplastic prepregs for temperatures ranging between 70 to 120 and concluded that increasing temperature decreases tensile modulus, reduces yield strength/strain, and increases the ductility of samples. Han and Chang [14] performed the uniaxial tensile test to evaluate the warp and weft behavior of uncured woven fabric prepreg based on the standard method ASTM D5035. Prior research has extensively investigated the behavior of short, thin-walled channel-section columns made of carbon/epoxy laminates under compressive loads using experimental and numerical methods [15–17]. Notably, Wysmulski [17] developed numerical models that accurately analyze the post-buckling response of composite structures, considering the impact of compressive load eccentricity. However, there seems to be no detailed study on the tensile behavior of unidirectional carbon epoxy prepreg considering the initial fiber waviness of tow and temperature effects on the tensile modulus.

Fiber waviness is one aspect of the unidirectional prepreg that can affect material properties and performance. The fiber alignment in the prepreg is a source of variability between samples and needs to be addressed when studying the mechanical behavior of UD prepregs [18]. Fiber waviness is any angle of misalignment in the fibers along the lamina's fiber direction (1 direction). Due to the viscous matrix, fibers can move between each other, which disrupts their alignment. Several studies have been carried out concerning the effects of fiber waviness on the material properties of composite materials and how to measure waviness [11,19–28], which can be grouped into experimental, analytical, and finite element approaches. Alves et al. performed an enhanced review of the defects of fiber waviness generated during fiber-reinforced polymer composites manufacturing [29].

Numerical micromechanical analysis is a useful method for modeling and studying the properties of heterogeneous materials, especially those with periodic microstructures. It involves defining a representative unit cell and applying periodic boundary conditions. Material properties are incorporated at the constituent level to represent the microstructure. These models are valuable for parametric material studies. Finite elements are used for analysis due to the complexity of the unit cell analysis with enforced constraints and boundary conditions. Garnich, Karami, and their collaborators [5,27,30,31] conducted comprehensive numerical studies on laminates with wavy fibers using linear elastic 3D FEA models of periodic sinusoidal unit cells. They investigated the effects of amplitude-to-wavelength ratio and fiber volume fraction on volume-averaged stress and strain. The results highlighted the importance of local stresses in predicting failure and the strong influence of fiber waviness on material stiffness. They compared localized stresses in wavy periodic unit cells with explicitly modeled fibers to straight homogeneous unit cells with introduced wavy fibers. The equivalence of the two models was demonstrated in linear elastic analysis. Furthermore, they examined the thermoelastic responses of composites by conducting FEA on wavy periodic unit cells with different amplitude-to-wavelength ratios and volume fractions. Their subsequent work involved FEA analysis of a straight unit cell with implicitly modeled localized fiber waviness, which revealed a significant

reduction in the strength of composite structures. Kuksenko et al. [26] investigated the large deformation response of composites reinforced by continuous wavy fibers using three-dimensional finite element analysis. An et al. [32] developed an RVE analysis plug-in tool in Abaqus/CAE to predict the effective orthotropic viscoelastic properties of unidirectional composites by taking as input the microstructure geometry and known properties of fibers and matrix. However, they did not cover the effect of fiber waviness on the tensile behavior of prepregs.

The main novelty of this work was to propose an RVE model that provides an evaluation of the effective properties of unidirectional carbon epoxy prepreg tow with waved fiber. Having obtained the stiffness matrix parameters of the tow, we also show how these properties are changed by the waviness ratio and fiber arrangement and can be used to explain the nonlinear tensile behavior of the towpreg. The results of this study can be applied to process modeling of AFP manufacturing to reduce the number of defects occurring in the process due to the instability of applied tensile loads.

## 2. Materials and Methods

### 2.1. Tensile Test

The objective of conducting tensile tests was to analyze the non-linear region of the stress/strain curve, with a particular focus on loads around 25 N, as these loads are most relevant to AFP and ATL manufacturing processes. Additionally, there is limited clarity regarding the underlying mechanism responsible for the nonlinearity observed in the modulus. It was hypothesized that the initial waviness of the fibers (assumed to follow a sinusoidal function) and the movement of fibers within the viscous epoxy matrix contributed to the non-linear behavior during tensile loading. The primary goals of the tensile testing were to quantify this theory regarding the cause of nonlinearity, propose a standardized test method for performing tensile tests on uncured prepreg, and gather data on the tensile modulus for comparison with finite element analysis (FEA) results. This data would serve as the basis for developing a representative volume element (RVE) model of composite material with waved fibers.

A unidirectional carbon/epoxy prepreg (Solvay S.A, CYCOM 977-2) supplied by Bombardier inc., Montreal, Canada was used for the tensile test. Table 1 summarizes the characteristics of the UD prepreg. Samples were cut from the prepreg, which was received in the form of a spool containing narrow and continuous strips. Before conducting the test, the samples were kept at room temperature for 1 h.

**Table 1.** Material properties of CYCOM 977-2 [33].

Fiber	Resin	Resin Content (%)	Tow Width (mm)	Tow Thickness (mm)
12K HTS-196	CYCOM 977-2	40	6	0.2

The uniaxial tests were performed using a HOSKIN tensile testing machine in tension mode, equipped with a 1 kN load cell and standard knurled grips, as illustrated in Figure 1. As the focus of the study was not on sample failure, a higher-rated load cell was not required. To provide heat during the tests, an IR lamp was utilized as a heat source. Additionally, the temperature of the specimen was measured using an infrared camera (FLIR T450c, FLIR, US).

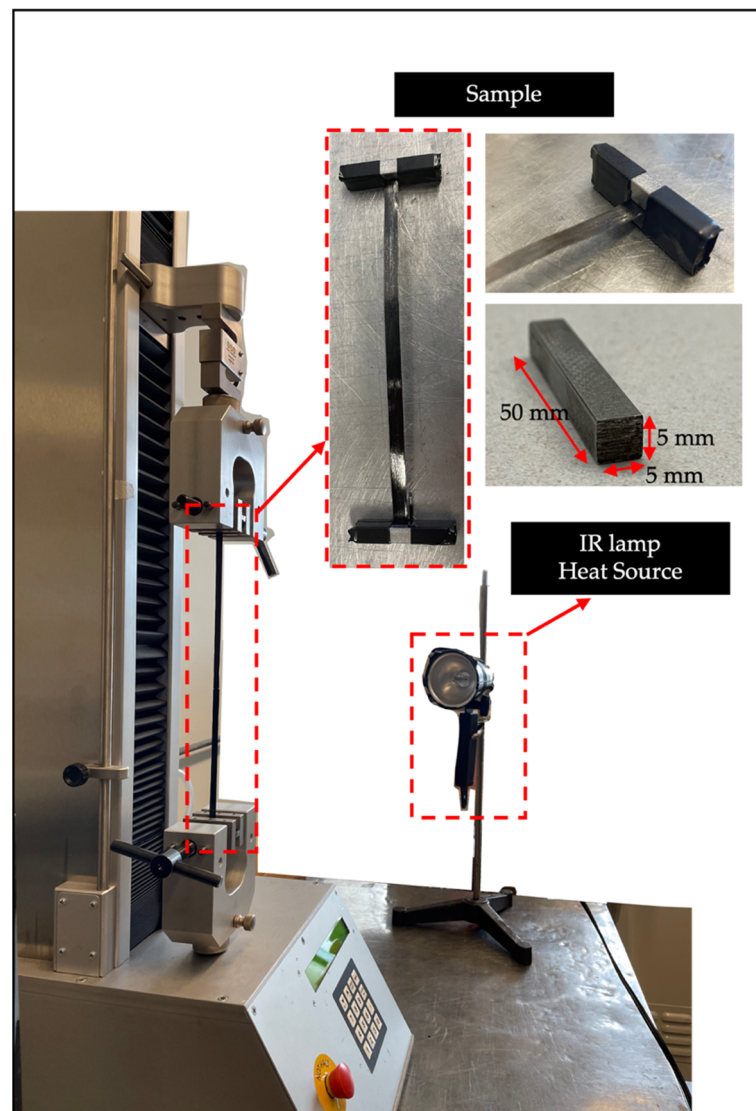


**Figure 1.** Tensile test setup.

In order to address the issue of slippage caused by the viscous nature of the uncured prepreg, the standard gripping method had to be modified. Several approaches have been developed to prevent slippage in the grips, including rapidly curing the ends of the specimens using heater plates [10], wrapping the grips in sandpaper to add an extra source of friction in holding the viscous sample [13], and wrapping the sample ends around the pins [1]. In this study, a specific gripping method was employed. The ends of the prepreg samples were wrapped around one of the steel rods approximately two times, equivalent to approximately 8 cm of material. The wrapped ends were then pressed against the other rod to create a sandwich-like arrangement. The steel bars used had a length of 50 mm and a cross-section of 5 mm × 5 mm. To ensure proper alignment and application of tensile load in the fiber direction, the samples were first set up and clamped in the lower grip. They were then carefully aligned and secured in the upper grip, taking precautions to avoid any misalignment in the sample setup.

## 2.2. Tensile Test Validation

Each sample underwent two testing runs to ensure reliable results. The primary objective of the first run was to establish system stability, validate the gripping technique, and apply a pre-load to the sample. This initial run followed standard tensile testing procedures, gradually increasing the load up to a maximum of 100 N at a displacement

rate of 2 mm/min. Once the first run concluded, the specimen was carefully returned to its original position, and the load was removed. After resetting the sample, the second run was conducted, aiming to reach a maximum allowable force of 200 N. The analysis of the tensile behavior encompassed the results obtained from this second tensile test run.

The influence of gauge length on tensile response was investigated to find the best possible gauge length. Tensile tests were conducted at room temperature using samples with varying gauge lengths within the range of 100 to 350 mm. The engineering stress and engineering strain values were computed based on the recorded force and displacement measurements during the experimental procedure. During the tests, it was observed that the outer edges of the sample did not experience tension during the loading process. To ensure the accuracy of the test results, the outer edges were removed by cutting, as depicted in Figure 2. Furthermore, it was assumed that the contribution of the uncured epoxy to the tensile modulus was insignificantly small. As a result, it was considered that the entirety of the stress was solely exerted on the fibers. This assumption was supported by the equation of the rule of mixtures (Equation (1)) commonly employed in determining the elastic modulus:

$$E_c = E_f V_f + E_m (1 - V_f) \quad (1)$$

where  $V_f$  and  $E_f$  are the fiber volume fraction and elastic modulus,  $E_m$  represents the modulus of the resin, and  $E_c$  is the combined elastic modulus. The rule of mixtures is derived from a constant-strain analysis, and it can be used to estimate the upper-bound of the modulus for a composite system. In this study, the fibers possessed an elastic modulus ( $E_f$ ) of 237 GPa, while the matrix had an elastic modulus ( $E_m$ ) of 3 GPa. As a result, with a volume fraction ( $V_f$ ) of 60%, the lamina exhibited a modulus of 143 GPa. Considering the viscous nature of the matrix, it was justified to assume that the modulus of the epoxy had a negligible contribution to the modulus of the tow. Thus, when calculating the stress within the sample, the width and thickness of the samples were adjusted based on the volume fraction of the fibers.

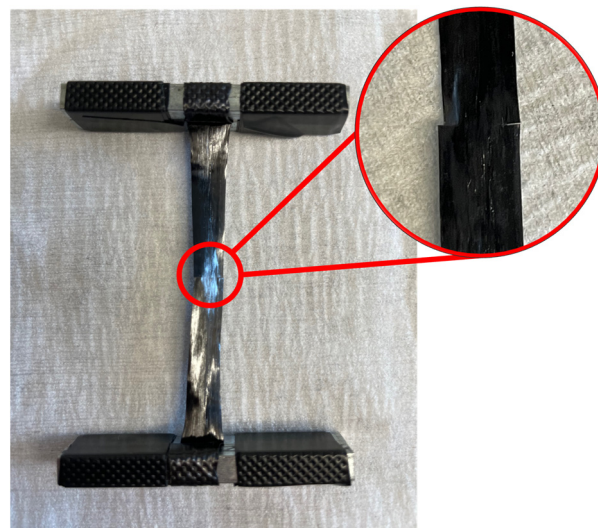


**Figure 2.** Width reduction of the sample.

It was anticipated that the impact of slippage would diminish with increasing gauge lengths. As the length of the sample was extended, the linear segments of the stress–strain curves converged to a single slope, as illustrated in Figure 3. The slopes of the stress–strain curves for longer gauge lengths in the linear region aligned with the expected tensile modulus predicted by the rule of mixtures. Since the experimental values closely approached 143 GPa, it was inferred that the influence of slippage was insignificant for specimen lengths equal to or greater than 300 mm. Consequently, tensile tests were performed using a gauge length of 300 mm, employing an average of eight samples. Table 2

summarizes the moduli for the gauge lengths. However, it was expected that there would be a discrepancy between the modulus values of cured and uncured samples. Cured prepreg experiences the effects of pressure and temperature, which can to some extent correct the waviness in the prepreg. On the other hand, waviness cannot be corrected during uncured tensile testing. Nevertheless, the resulting plots exhibited a linear trend across all samples, indicating that if there were any slippage within the grips, it would have resulted in non-linearity. Therefore, the proposed test method demonstrated good repeatability among the test samples, and the modification made to the grips proved effective in preventing sample slippage.

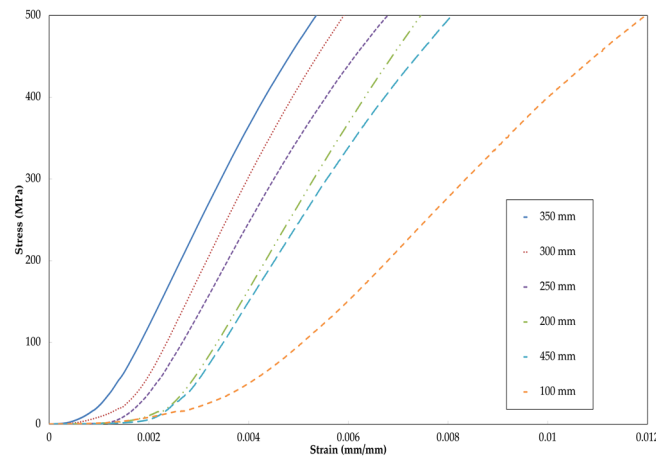


**Figure 3.** Tensile behavior of various gauge lengths tested under ambient conditions.

**Table 2.** Elastic modulus of various gauge lengths.

Gauge Length (mm)	Elastic Modulus (GPa)
100	62
150	97
200	101
250	108
300	130
350	130

### 3. Finite Element Model

This study employed finite element analysis (FEA) to assess the homogenized properties of a prepreg material featuring a periodic microstructure composed of cylindrical fibers arranged in sinusoidal paths. In the existing body of literature [32,34,35], analytical and numerical methods have been extensively employed to assess the effective elastic properties of unidirectional composites comprised of elastic matrix and fibers via the utilization of representative volume element (RVE) analysis. In this study, a Python code was developed to replicate these approaches to evaluate the properties for the prepreg tow with wavy fibers and including three steps, as follows.

#### 3.1. Create RVE

Three different fiber arrangements, namely, square, diamond, and hexagonal, were represented by developing three representative volume element (RVE) models using the Abaqus/CAE 2022 commercial software. The RVE model with a square arrangement is depicted in Figure 4. The geometrical parameters under consideration included the wavelength ( $\lambda$ ), amplitude ( $A$ ), and fiber diameter ( $d$ ). The directions  $z$ ,  $x$ , and  $y$  corresponded to the longitudinal, transverse within the plane of fiber waviness, and transverse normal to the plane of waviness directions, respectively.

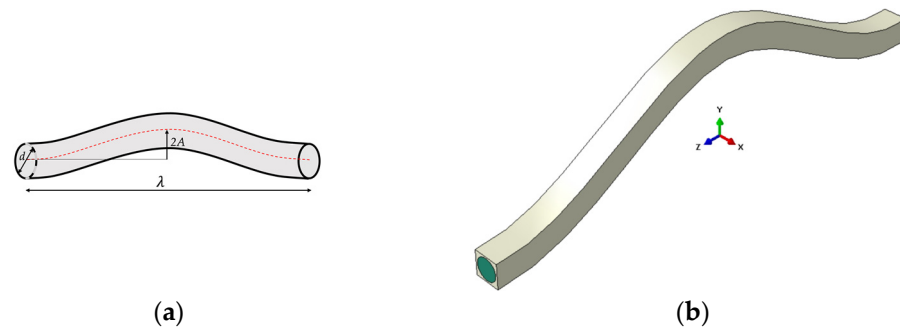


**Figure 4.** (a) Geometry of the wavy fiber. (b) RVE model with square arrangement.

The fiber material was assumed to be isotropic and elastic, characterized by an elastic modulus of 237 GPa and a Poisson’s ratio of 0.3. On the other hand, the matrix material was considered to be an isotropic and linear elastic material, with a Young’s modulus assigned a value of 3.5 GPa to represent a cured epoxy system [27]. As a result, the prepreg material exhibited orthotropic behavior.

3.2. Applied Periodic Boundary Conditions

The core principle of the RVE homogenization method involves numerically evaluating the response of a microscale RVE subjected to simple deformation. It is assumed that the RVE is a representative portion of a periodic material. Therefore, to maintain the periodicity of the RVE’s external surfaces during the deformation process, periodic boundary conditions (PBCs) must be applied. This is achieved by pairing opposite faces of the RVE and enforcing a constraint equation:

$$\begin{aligned}
 u_i(a_1, x_2, x_3) - u_i(-a_1, x_2, x_3) &= 2a_1\varepsilon_{i1}^0 & -a_1 \leq x_1 \leq a_1 \\
 u_i(x_1, a_2, x_3) - u_i(x_1, -a_2, x_3) &= 2a_2\varepsilon_{i2}^0 & -a_2 \leq x_2 \leq a_2 \\
 u_i(x_1, x_2, a_3) - u_i(x_1, x_2, -a_3) &= 2a_3\varepsilon_{i3}^0 & -a_3 \leq x_3 \leq a_3
 \end{aligned}
 \tag{2}$$

where  $2a_1$ ,  $2a_2$ , and  $2a_3$  are the lengths of the RVE model in the  $z$ ,  $x$ , and  $y$  directions, respectively, and  $\varepsilon^0$  is the uniform strain applied on the unit cell of the composite material.

Periodic boundary conditions in the RVE can be established by connecting opposite faces using constraint Equation (2). This equation excludes edges and vertices from the faces to prevent redundancy. The Python code developed facilitates the generation of periodic boundary conditions on the RVE model, utilizing coupling constraint equations (referred to as CE in Abaqus) to enforce the desired conditions.

In general, to write the CEs, one needs to define a reference point and master and slave nodes. Then, the master and slave nodes are connected by constraint equations representing PBCs. As noted earlier, the equations for the vertices, edges, and faces are dealt with separately from each other. The reference point is a dummy node and not connected to any part of a model; however, it can have arbitrary coordinates. One must define a load step to apply a defined value of displacement or strain as a boundary condition. Besides the CE equations, the following boundary conditions were enforced to prevent numerical singularity associated with rigid body motions. The central node at the center of the RVE was fixed in all directions. To prevent translations and rotations, the center nodes at the front and back faces were fixed in directions  $x$  and  $y$ .

In the context of finite element FE analysis, meshing is an important step that involves dividing a computational domain into a collection of smaller, interconnected elements. The quality of the mesh directly affects the accuracy and reliability of the numerical solution obtained from the FE analysis. Additional restrictions are imposed on the mesh when dealing with representative volume elements RVEs. One such restriction is the imposition of periodic boundary conditions; to impose periodic boundary conditions on an RVE, the paired faces that correspond to the periodic boundaries must be tessellated identically.

This means that the mesh on these paired faces should be the same or highly similar. One approach to achieve this is the SWEEP technique in Abaqus. The RVE model was meshed by C3D8R elements, as shown in Figure 5.

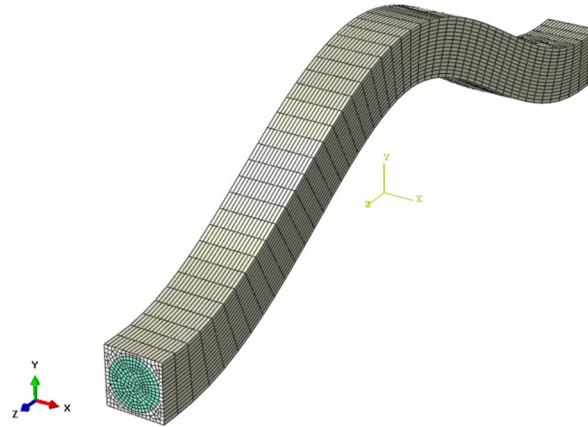


Figure 5. Finite element model of the RVE.

### 3.3. Homogenization Method

The application of strain  $\epsilon_{ij}^0$  at the boundary leads to a complex internal strain state within the RVE. Nevertheless, the average strain within the RVE, as demonstrated in Equation (3), is equal to the applied strain.

$$\bar{\epsilon}_{ij} = \frac{1}{V} \int_V \epsilon_{ij} dV = \epsilon_{ij}^0 \tag{3}$$

where  $V$  is the volume of the RVE. The stiffness matrix for an orthotropic material is:

$$\begin{Bmatrix} \bar{\sigma}_1 \\ \bar{\sigma}_2 \\ \bar{\sigma}_3 \\ \bar{\sigma}_4 \\ \bar{\sigma}_5 \\ \bar{\sigma}_6 \end{Bmatrix} = \begin{bmatrix} C_{11} & C_{12} & C_{13} & 0 & 0 & 0 \\ C_{12} & C_{22} & C_{23} & 0 & 0 & 0 \\ C_{13} & C_{23} & C_{33} & 0 & 0 & 0 \\ 0 & 0 & 0 & C_{44} & 0 & 0 \\ 0 & 0 & 0 & 0 & C_{55} & 0 \\ 0 & 0 & 0 & 0 & 0 & C_{66} \end{bmatrix} \begin{Bmatrix} \bar{\epsilon}_1 \\ \bar{\epsilon}_2 \\ \bar{\epsilon}_3 \\ \bar{\gamma}_4 \\ \bar{\gamma}_5 \\ \bar{\gamma}_6 \end{Bmatrix} \tag{4}$$

The entries in the stiffness tensor  $C_{ij}$  can be determined through a series of loads in which a constant average strain is applied to the homogenized RVE and then the average stress is measured:

$$\bar{\sigma}_\alpha = C_{\alpha\beta} \bar{\epsilon}_\beta \tag{5}$$

where  $\alpha, \beta = 1 \dots 6$ . So, the components of the stiffness tensor  $C$  are determined by solving six elastic models of the RVE subjected to the PBCs by Equation (2), where only one component of the strain is different from zero for each of the six problems. The elastic behavior of the RVE is analyzed with linear static analysis (\*Static, General in Abaqus) by considering the six loading cases, as listed in Table 3.

Table 3. Six loading cases and calculation of the elastic stiffness matrix  $C_{ij}$ .

	Loading Case	Calculation of $C_{ij}$
(a)	$\epsilon_{22}^0 = 1, \epsilon_{11}^0, \epsilon_{33}^0, \gamma_{23}^0, \gamma_{13}^0, \gamma_{12}^0 = 0$	$C_{12} = \bar{\sigma}_{11}, C_{22} = \bar{\sigma}_{22}, C_{23} = \bar{\sigma}_{33}$
(b)	$\epsilon_{33}^0 = 1, \epsilon_{11}^0, \epsilon_{22}^0, \gamma_{23}^0, \gamma_{13}^0, \gamma_{12}^0 = 0$	$C_{13} = \bar{\sigma}_{11}, C_{23} = \bar{\sigma}_{22}, C_{33} = \bar{\sigma}_{33}$
(c)	$\epsilon_{11}^0 = 1, \epsilon_{22}^0, \epsilon_{33}^0, \gamma_{23}^0, \gamma_{13}^0, \gamma_{12}^0 = 0$	$C_{11} = \bar{\sigma}_{11}, C_{12} = \bar{\sigma}_{22}, C_{13} = \bar{\sigma}_{33}$
(d)	$\gamma_{23}^0 = 1, \epsilon_{11}^0, \epsilon_{22}^0, \epsilon_{33}^0, \gamma_{13}^0, \gamma_{12}^0 = 0$	$C_{44} = \bar{\sigma}_{23}$
(e)	$\gamma_{12}^0 = 1, \epsilon_{11}^0, \epsilon_{22}^0, \epsilon_{33}^0, \gamma_{13}^0, \gamma_{23}^0 = 0$	$C_{55} = \bar{\sigma}_{13}$
(f)	$\gamma_{13}^0 = 1, \epsilon_{11}^0, \epsilon_{22}^0, \epsilon_{33}^0, \gamma_{12}^0, \gamma_{23}^0 = 0$	$C_{66} = \bar{\sigma}_{12}$

## 4. Results and Discussion

### 4.1. Experiment Results from Tensile Test

A total of eight samples were subjected to the testing procedure developed based on the evaluation of the test method. The testing process for each specimen consisted of two separate runs of tensile testing. The first run served to apply a pre-load to the sample, ensuring the stability of the system and verifying proper alignment and setup of the grips. After the completion of the first run, the sample was returned to its initial position, and a few seconds later, the second run of tensile testing was conducted. The results obtained from the second run of tensile testing were included in the analysis of the tensile behavior.

Plots were generated using the average data obtained from the experimental samples. These plots provided insights into the non-linear and final linear stiffness exhibited by the uncured prepreg material. Figure 6 illustrates the stress–strain curve derived from the average results of all the experiments conducted. The findings indicated that the tensile response of the uncured carbon fiber initially exhibited a non-linear behavior, followed by a linear region. Similar observations have been reported in previous studies, where the non-linear region is referred to as the lead-in region of the reduced modulus [1,10,12,13]. In our prepreg material, the lead-in (non-linear) region of the stress–strain curve extended up to 0.2% strain, after which a linear trend was observed.

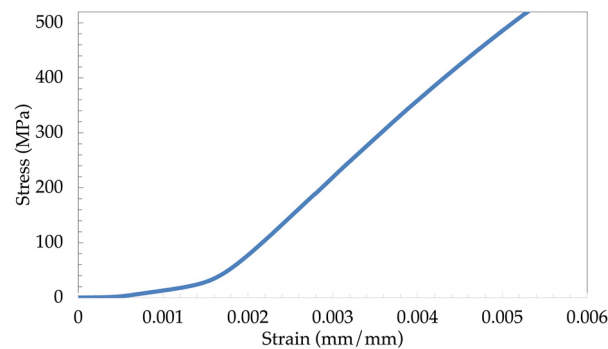


**Figure 6.** Average experimental results of the tensile behavior of uncured prepreg.

A linear trendline fitted to the linear region of the average stress–strain plot (0.2–0.5% strain) yielded a slope of 131, corresponding to an average linear modulus of 131 GPa. This value aligned closely with the linear modulus obtained in Section 2.2, which was reported as 130 GPa. The consistency in the linear modulus underscored the repeatability of the test method across the sample size. The experimentally determined values for the linear tensile modulus of each individual sample can be found in Table 4. The average linear tensile modulus of the uncured carbon fiber prepreg tested in this study was approximately 135 GPa with a standard deviation of 6 GPa. While this average value provided a general representation, it is important to note that individual samples were expected to exhibit a linear tensile modulus within the range of 130–142 GPa.

**Table 4.** Linear tensile modulus of each sample.

Sample Number	Linear Tensile Modulus (GPa)
Sample 1	130
Sample 2	140
Sample 3	130
Sample 4	132
Sample 5	136
Sample 6	141
Sample 7	138
Sample 8	135

The non-linearity region, ranging from 0% to 0.2% strain and ending at a load of approximately 30 N, holds significant importance in AFP and ATL manufacturing processes. These processes typically involve loads that fall within this region of non-linear stiffness. Although it is challenging to directly measure the loads during AFP and ATL, it is expected that the tensile modulus of uncured prepreg will lie within the non-linear region of its stress–strain response. Consequently, modeling the manufacturing process must account for factors such as waviness, misalignment, and the changing modulus within this region.

The experimental findings indicated that the waviness of the fibers plays a pivotal role in influencing the mechanical behavior of the uncured prepreg. The non-linear stress–strain curve arises from the interaction between the fiber waviness and the viscous matrix. The resistance encountered by the fibers as they are pulled through the resin leads to a reduction in stiffness. Additionally, the amplitude of the geometric waveform affects the stiffness as it alters the angle of the fibers, following the principles of classical lamination theory.

According to classical lamination theory, the modulus of composites is directly associated with the orientation of the fibers. Under the application of uniaxial tensile load, the viscous nature of the uncured epoxy matrix allows the fibers to align themselves with the loading direction. As the load and displacement increase, the alignment of the fibers becomes more closely aligned with the 0-degree direction (the direction of the applied load), resulting in a higher modulus. Eventually, as the load and displacement reach a critical point, the majority of the fibers will have their misalignment corrected, leading to a linear tensile response.

To determine the tensile modulus in the non-linear region, a curve fitting approach was employed. Firstly, the average plot across all samples was considered, and a second-order polynomial was utilized to fit a trendline to the range of 0% to 0.2% strain, as shown in Figure 7. The slope of the trendline was obtained by calculating the first derivative of the polynomial equation, which corresponds to the average tensile modulus exhibited by the uncured prepreg at a specific point within the non-linear region. To gain a clearer understanding of the tensile response in the non-linear region, the curve was divided into smaller sections, as illustrated in Figure 8. The equations for each trendline are visible on the curve, and the slope of the trendline represents the tensile modulus of the uncured prepreg. Applying these trendlines to each test sample, the average tensile modulus per section was determined in Table 5.

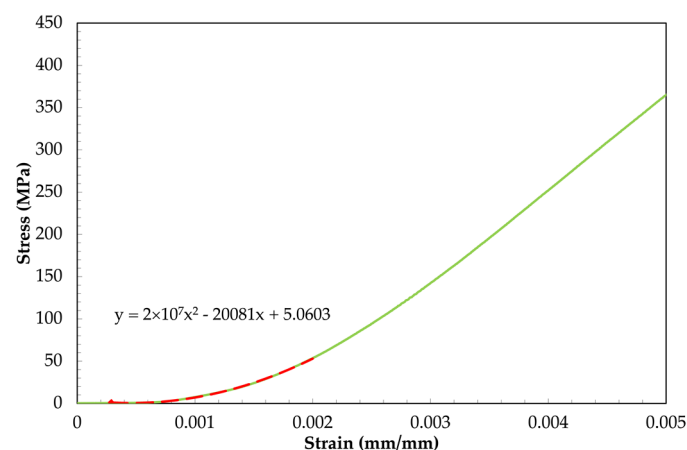


**Figure 7.** Trendline fit to the non-linear region.

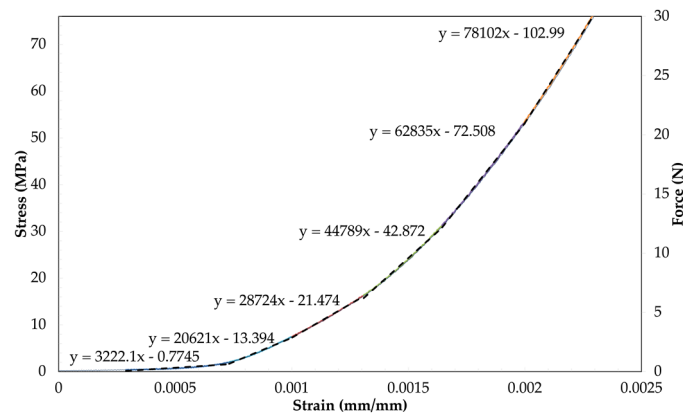


Figure 8. Linear trendline fit to non-linear region.

Table 5. Tensile moduli in non-linear region.

Section Number	Tensile Range (N)	Average Tensile Modulus (GPa)
1	1–3	20
2	3–6	29
3	6–12	45
4	12–20	63
5	20–30	78

#### 4.2. Effects of Temperature on the Tensile Behavior

The tensile behavior of the prepreg at room temperature revealed that the presence of waviness in the carbon fibers embedded in the viscous matrix contributed to the occurrence of the non-linear region. Considering the influence of temperature on the mechanical performance of the uncured epoxy matrix, the tensile tests were conducted at elevated temperatures using the same gripping solution as in the room temperature testing. Prior to testing, the samples were thawed at room temperature for 1 h after being removed from the freezer. The testing procedure involved applying an initial tensile load up to a maximum of 100 N, followed by returning the sample to its initial condition before conducting a second tensile test at the elevated temperature.

The results obtained from the tensile tests demonstrated that, at different temperatures, the prepreg samples exhibited a consistent slope in the linear region, confirming the assumption that the epoxy matrix’s contribution to stiffness in this region is negligible; see Figure 9. As was concluded in Section 3.1, the linear stiffness of the UD carbon epoxy prepreg was closely aligned with that of the fibers, and since the tensile modulus of the fibers remains independent of temperature, it can be inferred that the linear stiffness of the prepreg is unaffected by temperature variations. Furthermore, at higher temperatures, the viscosity of the epoxy matrix decreases, leading to reduced resistance to the movement of the prepreg. Despite this, on average, the fibers still need to move the same distance to rectify the waviness within the sample (straighten up). With less resistance to this movement, the stiffness plot is shifted upwards. The observed temperature effects on the reduction of the lead-in region during the tensile test aligned with previous findings on carbon epoxy prepreg [10].

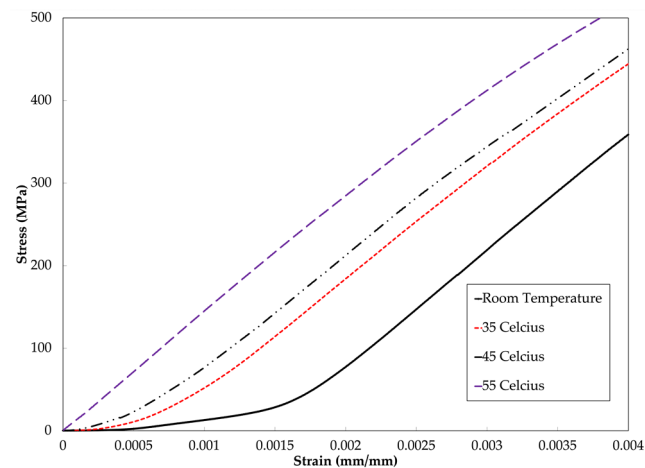


**Figure 9.** Engineering stress–strain curves from the tensile test at various temperatures.

#### 4.3. Finite Element Model

This section focuses on the computation of homogenized mechanical properties for composite materials with wavy fibers. The objective was to examine the impact of fiber waviness on prepreg properties. To achieve this, we analyzed three representative volume element (RVE) models associated with distinct fiber arrays: hexagonal, diamond, and square. These models were investigated within a waviness ratio range of 0 to 0.15, and the resulting homogenized stiffness matrix parameters were computed. The graphical representation of these parameters can be found in Figure 10. The results for the straight fiber agreed with [10,12,32,34], showing a slight difference in the three fiber arrangement models. For the effective Young's modulus  $E_1$ , longitudinal Poisson's ratio  $\nu_{12}$ , and longitudinal shear modulus  $G_{12}$ , the values predicted by the three models were all in excellent agreement with those noted for a random fiber distribution, which indicates that fiber arrangement had a negligible effect on these three effective longitudinal material properties. In contrast, for effective transverse material properties such as transverse Young's modulus  $E_2$ , transverse Poisson's ratio  $\nu_{23}$ , and shear modulus  $G_{23}$ , the values calculated by the hexagonal array agreed with the random fiber distribution, confirming that the random microstructure is well approximated by the hexagonal microstructure.

At lower levels of fiber waviness, there was a high level of agreement in the matrix stiffness parameters. However, as the waviness value exceeded 0.05, deviations started to emerge. These deviations were attributed to variations in the numerical discretization within each fiber array [26,30]. In summary, it can be inferred that fiber waviness has a significant impact on the longitudinal Young's modulus but has a negligible effect on other properties. As the degree of fiber waviness increases, the effective Young's modulus ( $E_1$ ) decreases, as observed in the results of the uniaxial tensile tests outlined in Section 3.2.

In accordance with previous discussions, the matrix and fibers were regarded as materials with linear elastic properties. To facilitate the examination of the temperature's impact on the behavior of the waved fiber, the representative volume element (RVE) model was employed, considering various matrix modulus values. This approach was chosen since temperature primarily affects the stiffness of the matrix, rather than that of the fibers. Figure 11 provides insights into the behavior of the RVE model with the square array at different temperatures, particularly in relation to the matrix stiffness. The figure indicates that, as the temperature increased, resulting in lower matrix stiffness values, the reduction in fiber waviness led to a more rapid change in the  $E_1$  values. This observation aligned well with the experimental results discussed in Section 3.2, further confirming the validity and applicability of the proposed RVE model. These results highlighted the significance of considering temperature effects on composite materials, specifically the influence of matrix stiffness, and emphasized the importance of accurately modeling and characterizing such phenomena for a comprehensive understanding of the material behavior.

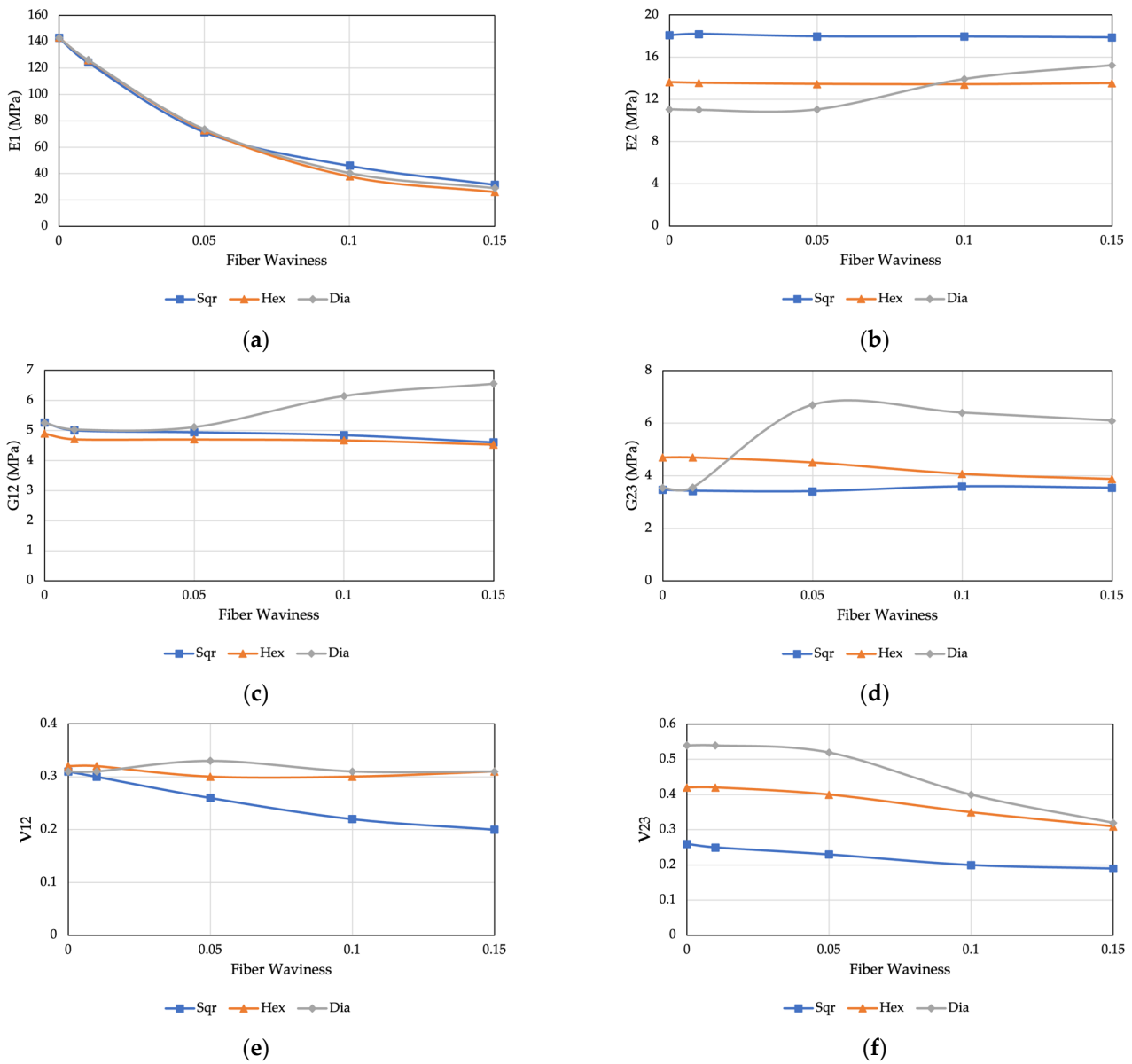


**Figure 10.** Effective elastic material properties according to the fiber waviness for hexagonal, diamond, and square arrays. (a) Longitudinal Young's modulus  $E_1$ , (b) transverse Young's modulus  $E_2$ , (c) shear modulus  $G_{12}$ , (d) shear modulus  $G_{23}$ , (e) Poisson's ratio  $\nu_{12}$ , and (f) Poisson's ratio  $\nu_{23}$ .

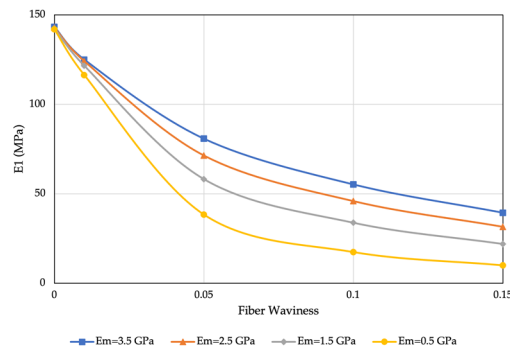


**Figure 11.** Effective longitudinal Young's modulus ( $E_1$ ) according to fiber waviness at different values of matrix stiffness.

## 5. Conclusions

This paper presented a comprehensive study of the tensile behavior of unidirectional carbon epoxy prepreg, combining both experimental and numerical approaches. Eight samples underwent two separate runs of tensile testing to assess their behavior. The stress–strain curves from the second run consistently showed a non-linear region followed by a linear region, in line with previous research. The average linear tensile modulus of the uncured carbon fiber prepreg was found to be approximately 135 GPa with a standard deviation of 6 GPa, closely matching the linear modulus of the fiber. According to classical laminate theory, individual samples are expected to exhibit a linear tensile modulus within the range of 130–142 GPa. Additionally, it was observed that the non-linear region, which holds significance for AFP and ATL manufacturing processes, occurred within the 0% to 0.2% strain range. The experimental findings shed light on the interaction between fiber waviness and the viscous matrix, leading to a reduction in stiffness. Furthermore, the amplitude of the geometric waveform played a role in impacting stiffness by influencing changes in fiber angle. Moreover, tensile tests conducted at different temperatures consistently showed a linear region with negligible stiffness contribution from the epoxy matrix within this range. The linear stiffness of the UD carbon epoxy prepreg closely mirrored that of the fibers and remained unaffected by temperature variations. However, at higher temperatures, the decreased viscosity of the epoxy matrix caused the stiffness plot to shift upward in the non-linear region. At the microscale, a Python code for numerical analysis was developed in Abaqus/CAE. This code enables the calculation of the orthotropic elastic properties of unidirectional prepreg with waved fibers, taking the microstructure geometry and the known properties of constituent materials as inputs. This study revealed that the arrangement of fibers had a negligible effect on the three effective longitudinal material properties. On the other hand, fiber waviness significantly impacted the longitudinal Young's modulus ( $E_1$ ), while it had a negligible effect on other properties. As the degree of fiber waviness increased, the effective Young's modulus ( $E_1$ ) decreased, as corroborated by the results from uniaxial tensile tests. Furthermore, this research demonstrated that higher temperatures and lower matrix stiffness values led to a more rapid change in  $E_1$  values as fiber waviness decreased. This alignment between numerical and experimental findings highlighted the capability of the proposed model to accurately predict the elastic properties of unidirectional composites with waved fibers.

**Author Contributions:** M.D.D.: Conceptualization, Methodology, Software, Validation, Formal analysis, Data curation, Writing—original draft, Writing—review and editing. M.C.: Conceptualization, Methodology, Formal analysis. M.H.: Conceptualization, Validation, Supervision, Project administration, Funding acquisition. All authors have read and agreed to the published version of the manuscript.

**Funding:** This research received no external funding.

**Data Availability Statement:** The Python codes proposed in this study are openly available at: <https://github.com/Mina-Derakhshani/Abaqus.git> (accessed on 19 July 2023).

**Acknowledgments:** The authors gratefully acknowledge financial support from the Natural Science and Engineering Research Council of Canada (NSERC) through a Discovery Grant.

**Conflicts of Interest:** The authors declare no conflict of interest.

## References

1. Dangora, L.M.; Mitchell, C.; White, K.D.; Sherwood, J.A.; Parker, J.C. Characterization of temperature-dependent tensile and flexural rigidities of a cross-ply thermoplastic lamina with implementation into a forming model. *Int. J. Mater. Form.* **2018**, *11*, 43–52. [[CrossRef](#)]
2. Rashidi, A.; Montazerian, H.; Yesilcimen, K.; Milani, A.S. Experimental characterization of the inter-ply shear behavior of dry and prepreg woven fabrics: Significance of mixed lubrication mode during thermoset composites processing. *Compos. Part Appl. Sci. Manuf.* **2020**, *129*, 105725. [[CrossRef](#)]
3. Kheradpisheh, M.; Hojjati, M. Wrinkle Formation and Initial Defect Sensitivity of Steered Tow in Automated Fiber Placement. *J. Compos. Sci.* **2021**, *5*, 295. [[CrossRef](#)]

4. Brasington, A.; Sacco, C.; Halbritter, J.; Wehbe, R.; Harik, R. Automated fiber placement: A review of history, current technologies, and future paths forward. *Compos. Part C Open Access* **2021**, *6*, 100182. [CrossRef]
5. Garnich, M.R.; Karami, G. Localized Fiber Waviness and Implications for Failure in Unidirectional Composites. *J. Compos. Mater.* **2005**, *39*, 1225–1245. [CrossRef]
6. Alshahrani, H.; Hojjati, M. A theoretical model with experimental verification for bending stiffness of thermosetting prepreg during forming process. *Compos. Struct.* **2017**, *166*, 136–145. [CrossRef]
7. Alshahrani, H.; Hojjati, M. Bending behavior of multilayered textile composite preregs: Experiment and finite element modeling. *Mater. Des.* **2017**, *124*, 211–224. [CrossRef]
8. Le, A.; Nimbalkar, S.; Zobeiry, N.; Malek, S. An efficient multi-scale approach for viscoelastic analysis of woven composites under bending. *Compos. Struct.* **2022**, *292*, 115698. [CrossRef]
9. Rajan, S.; Sutton, M.A.; Wehbe, R.; Gurdal, Z.; Kidane, A.; Emri, I. Characterization of viscoelastic bending stiffness of uncured carbon-epoxy prepreg slit tape. *Compos. Struct.* **2021**, *275*, 114295. [CrossRef]
10. Potter, K.; Langer, C.; Hodgkiss, B.; Lamb, S. Sources of variability in uncured aerospace grade unidirectional carbon fibre epoxy preimpregnate. *Compos. Part Appl. Sci. Manuf.* **2007**, *38*, 905–916. [CrossRef]
11. Potter, K.; Khan, B.; Wisnom, M.; Bell, T.; Stevens, J. Variability, fibre waviness and misalignment in the determination of the properties of composite materials and structures. *Compos. Part Appl. Sci. Manuf.* **2008**, *39*, 1343–1354. [CrossRef]
12. Zhang, W.; Ren, H.; Lu, L.; Zhang, Z.; Su, L.; Wang, Q.J.; Zeng, D.; Su, X.; Cao, J. Experimental Methods to Characterize the Woven Composite Prepreg Behavior during the Preforming Process. In Proceedings of the Thirty-First Technical Conference of the American Society for Composites 2016, Williamsburg, VA, USA, 19–21 September 2016. Available online: <https://www.osti.gov/biblio/1431017-experimental-methods-characterize-woven-composite-prepreg-behavior-during-preforming-process> (accessed on 29 November 2021).
13. Sentis, D.F.; Cochereau, T.; Orgéas, L.; Dumont, P.J.; Rolland du Roscoat, S.; Laurencin, T.; Terrien, M.; Sager, M. Tensile behaviour of uncured sheet moulding compounds: Rheology and flow-induced microstructures. *Compos. Part Appl. Sci. Manuf.* **2017**, *101*, 459–470. [CrossRef]
14. Han, M.-G.; Chang, S.-H. Draping simulations of carbon/epoxy fabric preregs using a non-orthogonal constitutive model considering bending behavior. *Compos. Part Appl. Sci. Manuf.* **2021**, *148*, 106483. [CrossRef]
15. Rozylo, P.; Falkowicz, K.; Wysmulski, P.; Debski, H.; Pasnik, J.; Kral, J. Experimental-Numerical Failure Analysis of Thin-Walled Composite Columns Using Advanced Damage Models. *Materials* **2021**, *14*, 6. [CrossRef]
16. Wysmulski, P.; Debski, H. The analysis of sensitivity to eccentric load of compressed thin-walled laminate columns. *AIP Conf. Proc.* **2019**, *2078*, 020006. [CrossRef]
17. Wysmulski, P. Non-linear analysis of the postbuckling behaviour of eccentrically compressed composite channel-section columns. *Compos. Struct.* **2023**, *305*, 116446. [CrossRef]
18. Zhou, X.-Y.; Qian, S.-Y.; Wang, N.-W.; Xiong, W.; Wu, W.-Q. A review on stochastic multiscale analysis for FRP composite structures. *Compos. Struct.* **2022**, *284*, 115132. [CrossRef]
19. Erice, B.; Thomson, D. Modelling the Non-linear fibre and matrix dominated compressive behaviour in unidirectional Fibre-reinforced composites. *Compos. Struct.* **2023**, *304*, 116396. [CrossRef]
20. Safdar, N.; Daum, B.; Rolfes, R. A numerical prediction of failure probability under combined compression-shear loading for unidirectional fiber reinforced composites. *Mech. Mater.* **2022**, *171*, 104352. [CrossRef]
21. Yurgartis, S.W. Measurement of small angle fiber misalignments in continuous fiber composites. *Compos. Sci. Technol.* **1987**, *30*, 279–293. [CrossRef]
22. Stewart, A.L.; Poursartip, A. Characterization of fibre alignment in as-received aerospace grade unidirectional prepreg. *Compos. Part Appl. Sci. Manuf.* **2018**, *112*, 239–249. [CrossRef]
23. Wilhelmsson, D.; Asp, L. A high resolution method for characterisation of fibre misalignment angles in composites. *Compos. Sci. Technol.* **2018**, *165*, 214–221. [CrossRef]
24. Joyce, P.J.; Kugler, D.; Moon, T.J. A Technique for Characterizing Process-Induced Fiber Waviness in Unidirectional Composite Laminates-Using Optical Microscopy. *J. Compos. Mater.* **1997**, *31*, 1694–1727. [CrossRef]
25. Herráez, M.; González, C.; Lopes, C.S.; de Villoria, R.G.; Llorca, J.; Varela, T.; Sánchez, J. Computational micromechanics evaluation of the effect of fibre shape on the transverse strength of unidirectional composites: An approach to virtual materials design. *Compos. Part Appl. Sci. Manuf.* **2016**, *91*, 484–492. [CrossRef]
26. Kuksenko, D.; Böhm, H.J.; Drach, B. Effect of micromechanical parameters of composites with wavy fibers on their effective response under large deformations. *Adv. Eng. Softw.* **2018**, *121*, 206–222. [CrossRef]
27. Garnich, M.R.; Karami, G. Finite Element Micromechanics for Stiffness and Strength of Wavy Fiber Composites. *J. Compos. Mater.* **2004**, *38*, 273–292. [CrossRef]
28. Chanda, A.; Sinha, S.K.; Datta, N.V. The influence of fiber alignment, structure and concentration on mechanical behavior of carbon nanofiber/epoxy composites: Experimental and numerical study. *Polym. Compos.* **2021**, *42*, 1155–1173. [CrossRef]
29. Alves, M.P.; Cimini, C.A., Jr.; Ha, S.K. Fiber waviness and its effect on the mechanical performance of fiber reinforced polymer composites: An enhanced review. *Compos. Part Appl. Sci. Manuf.* **2021**, *149*, 106526. [CrossRef]
30. Karami, G.; Garnich, M. Effective moduli and failure considerations for composites with periodic fiber waviness. *Compos. Struct.* **2005**, *67*, 461–475. [CrossRef]

31. Karami, G.; Garnich, M. Micromechanical study of thermoelastic behavior of composites with periodic fiber waviness. *Compos. Part B Eng.* **2005**, *36*, 241–248. [[CrossRef](#)]
32. An, N.; Jia, Q.; Jin, H.; Ma, X.; Zhou, J. Multiscale modeling of viscoelastic behavior of unidirectional composite laminates and deployable structures. *Mater. Des.* **2022**, *219*, 110754. [[CrossRef](#)]
33. CYCOM 977-2. Solvay. Available online: <https://www.solvay.com/en/product/cycom-977-2> (accessed on 29 November 2021).
34. Riaño, L.; Joliff, Y. An Abaqus<sup>TM</sup> plug-in for the geometry generation of Representative Volume Elements with randomly distributed fibers and interphases. *Compos. Struct.* **2019**, *209*, 644–651. [[CrossRef](#)]
35. Omairey, S.L.; Dunning, P.D.; Sriramula, S. Development of an ABAQUS plugin tool for periodic RVE homogenisation. *Eng. Comput.* **2019**, *35*, 567–577. [[CrossRef](#)]

**Disclaimer/Publisher’s Note:** The statements, opinions and data contained in all publications are solely those of the individual author(s) and contributor(s) and not of MDPI and/or the editor(s). MDPI and/or the editor(s) disclaim responsibility for any injury to people or property resulting from any ideas, methods, instructions or products referred to in the content.